Journal of Natural Gas Science and Engineering 34 (2016) 811–822

Contents lists available at ScienceDirect

Journal of Natural Gas Science and Engineering

journal homepage: www.elsevier.com/locate/jngse

Influence of high-pressure CO_2 exposure on adsorption kinetics of methane and CO_2 on coals

Qianqian Wang [a], Wei Li [a, b], Dengfeng Zhang [a, *], Haohao Wang [a], Wenping Jiang [c], Li Zhu [a], Jun Tao [a], Peili Huo [a], Jin Zhang [a]

[a] Faculty of Chemical Engineering, Kunming University of Science and Technology, Kunming 650500, PR China
[b] Department of Earth Science and Engineering, Taiyuan University of Technology, Taiyuan 030024, PR China
[c] Xi'an Research Institute of China Coal Technology & Engineering Group Corp., Xi'an 710077, PR China

ARTICLE INFO

Article history:
Received 23 February 2016
Received in revised form
28 June 2016
Accepted 14 July 2016
Available online 18 July 2016

Keywords:
Coal
Methane
CO_2 sequestration
High-pressure CO_2 exposure
Adsorption kinetics

ABSTRACT

This work was performed to address the effect of high-pressure CO_2 exposure on methane and CO_2 adsorption kinetics behavior on various rank coals. The adsorption kinetics curves of methane and CO_2 on coal samples before and after CO_2 exposure were measured under 45 °C and approximately 0.41 MPa. The possible reasons for CO_2 exposure dependence of adsorption kinetics of methane and CO_2 were also studied. The results show that CO_2 exposure causes a decrease in both methane and CO_2 diffusion-adsorption rates on coals as indicated by both macropore and micropore apparent diffusion coefficients. The decreasing trend of diffusion-adsorption rate is more evident for CO_2 than methane on coals after CO_2 exposure. Further investigations indicate that the effect of CO_2 exposure on adsorption kinetics of methane and CO_2 is related to both surface chemistry and pore structure of coals. On the one hand, pore structure analyses indicate that CO_2 exposure causes a slight decrease in micropore and meso/macropore of coals. On the other hand, CO_2 exposure leads to a decrease in the oxygen-containing functional groups mainly including carbonyl (−C=O) and carboxyl (−COOH) of coals. The oxygen-containing functional groups on coal surface benefit the diffusion and adsorption of CO_2. However, this effect is opposite for methane. Thus, it is concluded that the alterations of both pore structure and oxygen-containing functional groups due to CO_2 exposure contribute to the decrease of CO_2 diffusion-adsorption rate. With regard to methane, the influence of pore structure on adsorption kinetics behavior is superior to the oxygen-containing functional groups, which accounts for the decrease of the adsorption and diffusion rate. The design of practical CO_2-ECBM process needs to consider the effect of CO_2 exposure on methane and CO_2 diffusion and adsorption within coals.

1. Introduction

Global warming issues caused by carbon dioxide (CO_2), an anthropogenic greenhouse gas (GHG), are increasingly aggravating, which bring a series of negative effects to the natural ecosystem balance and human sustainable development (Lindzen, 1997). It is acknowledged that deep coal seams as a huge reservoir can store CO_2 in geologic time, which is considered as an effective way to mitigate CO_2 emissions (White et al., 2005). Coal is provided with complex pore morphology and special surface chemistry and thus has strong ability to adsorb gas molecules especially under higher reservoir pressure (Giroux et al., 2006; Green et al., 2011; Li et al., 2015; Nie et al., 2015). Theoretical and experimental methods have demonstrated that CO_2 adsorption capacity on coal is superior to methane. Thus, the coalbed methane resource can be recovered when CO_2 is injected and adsorbed on the coal matrix.

Hitherto, most investigations were carried out to study the adsorption-desorption behaviors of methane and CO_2 on coals under the reservoir conditions (Clarkson and Bustin, 2000; Mastalerz et al., 2004; Zhang et al., 2011b), displacement behavior of coalbed methane recovered by CO_2 injection (Prusty, 2008; Zhang et al., 2011c; Zhou et al., 2013), and coal matrix swelling phenomenon induced by CO_2 adsorption (Lin et al., 2008; Mazumder and Wolf, 2008; Shi et al., 2014). It is necessary to point

* Corresponding author. Kunming University of Science and Technology, No. 727 Jingming South Road, Chenggong District, Kunming City 650500, Yunnan Province, PR China.
E-mail address: plum0627@163.com (D. Zhang).

http://dx.doi.org/10.1016/j.jngse.2016.07.042
1875-5100/

out that complex interactions existed between CO_2 fluid and coal under the optimum reservoir conditions due to the unique physicochemical characteristics of the injected CO_2 fluid and coal itself. However, the studies on the complex interactions of CO_2 fluid with coal are relatively scarce. Both Kolak and Burruss (2006, 2014, Kolak et al., 2015) and our previous work (Zhang et al., 2013a) found that the injected CO_2 was supercritical fluid at the optimum sequestration depth and was capable of mobilizing alkane and polycyclic aromatic hydrocarbons (PAHs) dissociating in the macromolecular structure of coal. Cao et al. (2011) found that high-pressure CO_2 exposure caused an increase in the alkyl carbons and a decrease in aromaticity for vitrain and fusain, nevertheless this trend was opposite for clarain and bright clarain. Huang et al. (2014) reported that hydrogen bonds would be formed between CO_2 and the oxygen-containing functional groups on coal surface based on Density Functional Theory including dispersion correction (DFT-D) calculation. Our previous work studied high-pressure CO_2 exposure dependence of methane and CO_2 adsorption equilibrium behavior on coals and demonstrated that high-pressure CO_2 exposure led to an increase in the maximum methane adsorption capacity by 3.45%–10.37% and a decrease in the maximum CO_2 adsorption capacity by 9.99%–23.93% (Wang et al., 2015). Hitherto, the study related to the effect of CO_2 exposure operated at low-pressure ranging between 0.21 and 0.62 MPa on the adsorption rate of CO_2 has been reported (Goodman et al., 2006); however, the influence of high-pressure CO_2 exposure on adsorption kinetics of methane and CO_2 on coals is still unclear. The CO_2 injection rate and methane recovery efficiency of the practical CO_2-ECBM is partly limited by the ability of methane molecule and CO_2 molecule to diffuse in the coal seams (Lin et al., 2008; Siriwardane et al., 2009; Wong et al., 2007). Thus, in our work, an effort was made to investigate the effect of CO_2 exposure on the adsorption kinetics of methane and CO_2 on coals and the possible mechanism was also discussed in detail.

2. Experimental methods

2.1. Samples collection and preparation

Four coal samples collected from the main production areas of coal resources in China were used in this study. To avoid the undesired physical and chemical changes due to the atmospheric oxidation (Mastalerz et al., 2009), each coal sample was preserved in a sealed plastic bag filled with inert helium before use. The proximate analysis, the equilibrium moisture and the maximum vitrinite reflectance coefficient designated as $R_{o,max}$ of each coal were performed in our previous research (Wang et al., 2015). According to the analysis results shown in Table 1, HB, SM and ED are high-volatile bituminous coals, and YQ is classified as anthracite.

2.2. Exposure of coal to supercritical CO_2 fluid

In this work, the interaction of high-pressure CO_2 fluid with coals was performed on a Model SFE-500 dynamic extraction system supported by Thar Process, Inc., U.S.A. The experimental apparatus mainly comprised a pressure-charging unit, an extraction unit and a collection unit, as shown in Fig. 1. The pressure-charging unit was able to generate high-pressure CO_2 fluid up to 60 MPa by a P-series booster pump. The mass flow rate of CO_2 injected from the pressure-charging unit into the subsequent extraction unit could be regulated in the range between 0 and 30 g min^{-1}. The interaction of CO_2 with coal occured in the extraction unit which was previously loaded with coal sample. An automated back pressure regulator installed between the extraction unit and the collection unit was able to maintain constant pressure of the extraction unit. The extract phase released from the extraction unit could be gathered from the collection unit. Both the extraction unit and the collection unit were equipped with a heating jacket. The temperature of both the extraction unit and the collection unit could be regulated within a range from the ambient temperature to 150 °C. It was worth noting that Model SFE-500 extraction system was a dynamic process, and the extraction unit and the collection unit could be treated as the CO_2 injection well and methane recovery production well of CO_2-ECBM, respectively. Therefore, the conclusion derived from the interactions between CO_2 and coal operated on the SFE-500 extraction system was meaningful to the practical CO_2-ECBM.

Prior to the interaction test, all coal samples were carefully crushed and sieved to generate particles with size of 100–120 mesh and then dried at 105 °C for 24 h under vacuum condition. 100 ± 0.0005 g of each dry coal sample was weighed for the interaction of CO_2 with coal to meet the needs of subsequent physicochemical analyses and adsorption kinetics test. The mass flow rate of CO_2 injection and the duration of the interaction process were determined as 10 g min^{-1} and 12 h, respectively. Previous work showed that the optimum depth for geologic sequestration of CO_2 was around 800–1000 m (Orr, 2009), where the temperature and pressure of the stored CO_2 at this depth exceeded the critical parameters of CO_2, i.e. 31.05 °C and 7.38 MPa (Span and Wagner, 1996). Thus, the temperature and pressure of the interaction of CO_2 with coal were set as 45 °C and 12 MPa, respectively.

2.3. Adsorption kinetics test

In this work, volumetric method was used to measure the adsorption kinetics of methane and CO_2 on coals before and after CO_2 exposure. The operation temperature and pressure were 45 °C and 0.41 MPa, respectively. The frequency of data record was set as 1 s.

Previous work found that the measuring precision of temperature and pressure significantly affected the adsorption test (Sakurovs et al., 2009; Zhang et al., 2013b). Therefore, a natural convection air oven with temperature control precision of 0.1 °C (UNB500, Memmert GmbH & Co. KG, Germany), and pressure transducers with a super precision of 0.05% of the full scale 20 MPa (Super TJE, Honeywell International, Inc., U.S.A) were employed. The detailed apparatus information and experimental procedures could be found in the work of Wang et al. (2015). According to the

Table 1
Characteristics of each coal sample (Wang et al., 2015).

Sample	HB	SM	ED	YQ
Place of origin	Hulunbuir city	Yulin city	Erdos city	Yangquan city
Ash (dried basis), wt%	13.26	10.20	4.31	19.42
Volatile matter (dried basis), wt%	35.40	31.47	30.96	8.92
Fixed carbon (dried basis), wt%	51.35	58.34	64.73	71.68
Equilibrium moisture, wt%	18.18	9.73	11.93	5.31
$R_{o\ max}$, %	0.77	0.88	0.93	2.62

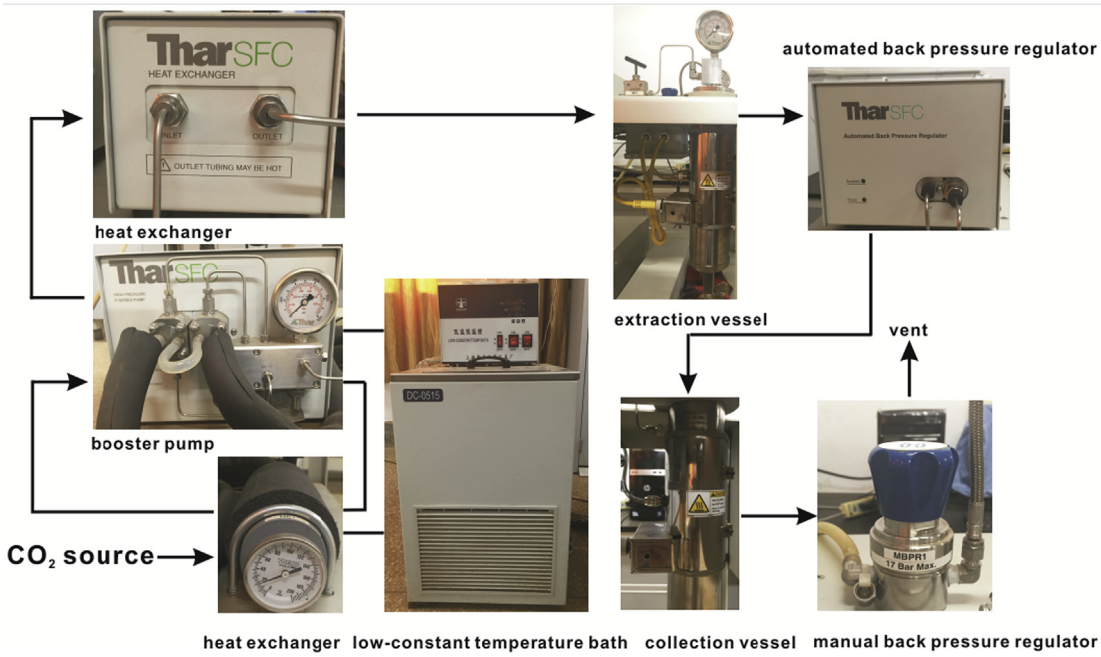

Fig. 1. Model SFE-500 dynamic extraction system.

time-based experimental records of pressure and temperature, the adsorption amounts of pure methane and CO_2 corresponding to any time (t) are calculated by:

$$\Delta GSE = \frac{1}{RmT}\left(\frac{P_2V_{RC}}{Z_2} + \frac{P_1V_V}{Z_1} - \frac{P_3V_{RC}}{Z_3} - \frac{P_4V_V}{Z_4}\right) \quad (1)$$

where GSE, i.e. the abbreviation of Gibbsian surface excess, is the experimental adsorption data, mmol g^{-1}; m is the mass of the coal sample, g; T is the operation temperature, K; R is the universal gas constant, 8.314 J mol^{-1} K^{-1}. P_1 and P_2 are the initial pressures of sample cell and reference cell, respectively, Pa; P_3 and P_4 are the pressures of reference cell and sample cell corresponding to t when the adsorption occurs, respectively, Pa. V_{RC} and V_V are the volume of the reference cell and the void volume of sample cell loaded with coal sample calibrated by helium, respectively. Z_1, Z_2, Z_3, and Z_4 are methane or CO_2 compressibility factors corresponding to P_1, P_2, P_3, and P_4 at temperature T, respectively. In this work, Wagner & Span-EoS and Span & Wagner-EoS with superior predictive accuracy were used to generate the compressibility factors (Z) of methane and CO_2, respectively (Wagner and Span, 1993; Span and Wagner, 1996). Prior to the adsorption kinetics test, all the samples before and after CO_2 exposure were entirely degassed under vacuum condition at 105 °C overnight. Each adsorption test was performed on 40 ± 0.0005 g of coal sample after drying process to study the effect of CO_2 exposure on the adsorption kinetics of methane and CO_2 on coals.

2.4. Pore structure characterization

Pore structures including micropore and meso/macropore were analyzed in our previous work (Wang et al., 2015). Micropore analysis by adsorption method using CO_2 as molecular probe at 273.15 K was performed on ASAP 2020 (Micromeritics instruments, U.S.A.). The micropore surface area and volume were obtained by Dubinin-Radushkevich (D-R) model (Gathitu et al., 2009).

The meso/macropore structure of coal sample was also given by ASAP 2020 (Micromeritics instruments, U.S.A.) using low temperature nitrogen adsorption-desorption method. The nitrogen adsorption and desorption isotherms at 77 K were collected at relative pressures (P/P_0) range between 0.005 and 0.995. The specific surface area and the pore volume of each sample were calculated using the Brunauer-Emmet-Teller (BET) model and Barrett-Joyner-Halenda (BJH) model, respectively (Viete and Ranjith, 2007; Yang, 2003).

Prior to micropore and meso/macropore analyses, all the coal samples before and after CO_2 exposure were fully degassed under vacuum for 12 h at 90 °C to effectively remove the residual gas and moisture.

2.5. FTIR analysis

EQUINOX 55 FTIR spectrometer (Bruker Corp., Germany) was used to determine the chemical properties of coals before and after CO_2 exposure. The dried spectroscopic pure potassium bromide (KBr) carrier and coal samples were fully pulverized and mixed at a mass ratio of 1:100, and then pressed into a pellet in a mold. The pellets were dried for 24 h under vacuum condition to decrease the contribution of water to the spectra. The spectra were obtained with a resolution of 4 cm^{-1}.

3. Modeling of adsorption kinetics

Hitherto, two types of models, i.e. the unipore diffusion model and the bidisperse diffusion model, are available to describe the fluid diffusion and adsorption behavior within the pore structure of coal.

The unipore model using a single parameter, i.e. effective diffusivity, assumed that the pore structure in the coal matrix was homogenous, which meant that the pore width was consistent. However, Gan et al. (1972), Yao et al. (2014) and Smith (1982) pointed out that spherical shaped macrospheres and uniform microspheres were present inside the coal matrix. Therefore, the unipore model failed to describe the gas diffusion behavior due to the bidisperse nature of coal. On the contrary, numerous works confirmed that the bidisperse diffusion model was successfully to

describe the methane and CO_2 diffusion and adsorption on coal (Cui et al., 2004; Ruckenstein et al., 1971; Smith and Williams, 1984). Thus, the bidisperse diffusion model was selected to the adsorption kinetics study in this work.

The simplified bidisperse model covers a fast macropore diffusion stage at the beginning of the experiment and a much lower micropore diffusion stage towards the end of the experiment period (Pan et al., 2010).

The model form corresponding to the fast phase is (Ruckenstein et al., 1971):

$$\frac{N_{\text{macro}}}{N_{\text{macro},\infty}} = 1 - \frac{6}{\pi^2}\sum_{n=1}^{\infty}\frac{1}{n^2}\exp\left(-\frac{D_{\text{macro}}n^2\pi^2 t}{R_{\text{macro}}^2}\right) \tag{2}$$

where N_{macro} and $N_{\text{macro},\infty}$ are the total amount of the diffusion gas in the macropore corresponding to time t and the equilibrium state, respectively, mmol g^{-1}. R_{macro} is the macropore radius, m, and D_{macro} is the macropore effective diffusivity, $m^2\ s^{-1}$.

The slow step of micropore diffusion stage is expressed as (Ruckenstein et al., 1971):

$$\frac{N_{\text{micro}}}{N_{\text{micro},\infty}} = 1 - \frac{6}{\pi^2}\sum_{n=1}^{\infty}\frac{1}{n^2}\exp\left(-\frac{D_{\text{micro}}n^2\pi^2 t}{R_{\text{micro}}^2}\right) \tag{3}$$

where N_{micro} and $N_{\text{micro},\infty}$ are the total amount of the diffusion gas in the micropore corresponding to time t and the equilibrium state, respectively, mmol g^{-1}. R_{micro} is the micropore radius, m, and D_{micro} is the micropore effective diffusivity, $m^2\ s^{-1}$.

The entire diffusion process uptake is given by:

$$\frac{N_t}{N_\infty} = \frac{N_{\text{macro}} + N_{\text{micro}}}{N_{\text{macro},\infty} + N_{\text{micro},\infty}} = \beta\frac{N_{\text{macro}}}{N_{\text{macro},\infty}+} + (1-\beta)\frac{N_{\text{micro}}}{N_{\text{micro},\infty}} \tag{4}$$

where β defined as the ratio of the amount of gas adsorption in macropore to the total adsorption is given by:

$$\beta = \frac{N_{\text{macro},\infty}}{N_{\text{macro},\infty} + N_{\text{micro},\infty}} \tag{5}$$

Substituting Eq. (2) and Eq. (3) into Eq. (4), the fitting parameters could be generated by nonlinear curve fitting method.

It is necessary to mention that the actual amount of adsorption, known as the absolute adsorption amount (N_{abs}), is used in adsorption kinetics study.

The relationship between GSE and N_{abs} is given by:

$$N_{\text{abs}} = \frac{\text{GSE}}{1 - \frac{\rho_b}{\rho_a}} \tag{6}$$

where ρ_b and ρ_a are the bulk density of the adsorbate and the density of the adsorbed phase, respectively. The adsorbed phase is always regarded as a pseudo-liquid state (Clarkson et al., 1997; Do and Do, 2003). Thus, the liquid densities of methane (0.421 g ml^{-1}) and CO_2 (1.227 g ml^{-1}) at the boiling point under the atmospheric pressure are designated as ρ_a of methane and CO_2, respectively (Harpalani et al., 2006; Siemons and Busch, 2007).

The bidisperse model is derived based on the assumption that the adsorption system has given rise to isotherm exhibiting linear shape (Ruckenstein et al., 1971). As shown in Figs. 2 and 3, all the isotherms based on N_{abs} of methane and CO_2 adsorption on coals before and after CO_2 exposure exhibit approximately linear feature. Therefore, the bidisperse model can be applied to describe the adsorption kinetics behavior in this work.

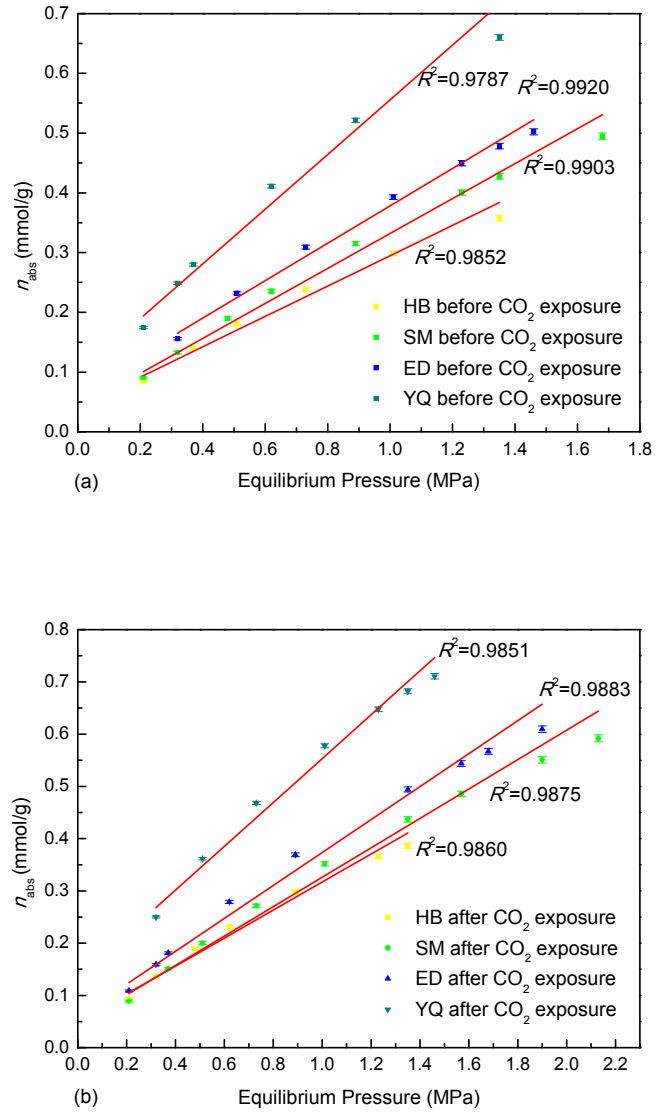

Fig. 2. Absolute adsorption isotherms (N_{abs}) of methane adsorption on various coals.

4. Results and discussions

4.1. Adsorption kinetics and the bidisperse model fitting

The raw pressure-versus-time of methane and CO_2 adsorption on coals before and after CO_2 exposure at 0.41 MPa and 45 °C are shown in the insets in Figs. 4 and 5, respectively. It can be found that although the diffusion and adsorption processes of methane and CO_2 on coals take a long time to reach the equilibrium state, all the pressure profiles show a rapid decrease within the initial 200 s when the adsorption occurs and then the adsorption process approaches to the equilibrium state gradually.

As can be seen in Figs. 4 and 5, each bidispere model fitting curve is well consistent with the experimental curve for both methane and CO_2 adsorption kinetics curves of coals before and after CO_2 exposure. It is also found from the bidisperse model fitting parameters listed in Tables 2 and 3 that the multiple correlation coefficients (R^2) of methane and CO_2 adsorption kinetics on various coals obtained from the bidisperse model are in the range of 0.8904–0.9883 and 0.9013–0.9696, respectively. Thus, the bidisperse model can well describe the adsorption kinetics of methane

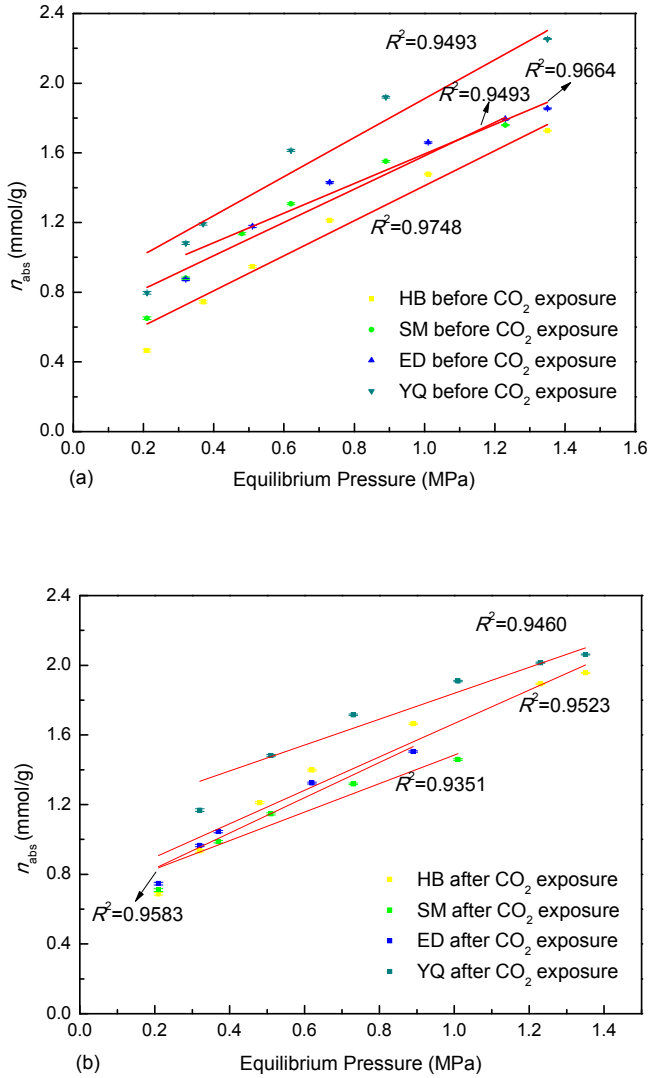

Fig. 3. Absolute adsorption isotherms (N_{abs}) of CO_2 adsorption on various coals.

and CO_2 on coals before and after CO_2 exposure.

Under the experimental conditions, the magnitude orders of methane and CO_2 apparent diffusion coefficient corresponding to macropore and micropore (defined as D_{macro}/R^2_{macro} and D_{micro}/R^2_{micro}, respectively) are 10^{-4}-10^{-3} and 10^{-5}-10^{-4}, respectively, which show a good agreement with the values reported from the previous investigations (Pan et al., 2010; Bhowmik and Dutta, 2013). Previous analysis indicates that an adsorbate molecule with the smaller kinetic diameter and larger adsorption energy has the greatest ability to diffuse into the pores of various sizes of the adsorbent (Cui et al., 2004). In comparison with methane (0.38 nm), the molecular kinetics diameter of CO_2 (0.33 nm) is smaller (Shieh and Chung, 1999). In addition, our previous study based on quantum chemistry calculation shows that the Lennard-Jones (6–12) potential well of CO_2 is deeper than that of methane (Wang et al., 2015). The above analyses may account for larger apparent diffusion coefficient of CO_2 than methane adsorption on the same coal sample shown in Tables 2 and 3. The β value defined in the bidisperse model shown in Eq. (5) is relatively large, which is consistent with the previous study (Clarkson and Bustin, 1999a; Pan et al., 2010). The experimental coal samples have been crushed (<100 mesh), and the intact pore, especially most macropore and macropore cleat may be destroyed. Therefore, the large β value means that a large number of gases are adsorbed not only in macropore, but also in accessible pores including micropore. Finally, it worth noting that CO_2 exposure has an enormous impact on the macropore and micropore apparent diffusion coefficients of methane and CO_2 in coal. Specially, except for the micropore apparent diffusivity of methane, CO_2 exposure causes a decrease in both macropore apparent diffusivity and micropore apparent diffusivity for methane and CO_2 adsorption on each coal sample. Moreover, the change of diffusivity of CO_2 (18.03%–49.68% and 22.00%–96.49% for macropore apparent diffusivity and micropore apparent diffusivity, respectively) due to CO_2 exposure is greater than that of methane (12.29%–45.11% and 33.33%–64.91% for macropore apparent diffusivity and micropore apparent diffusivity, respectively).

4.2. Mechanism of CO_2 exposure dependence of adsorption kinetics

Some of the earlier investigations have reported that the properties of adsorbate and adsorbent affect the adsorption kinetics behavior of methane and CO_2 on coal (Charrière et al., 2010; Gruszkiewicz et al., 2009; Busch et al., 2004). For a specific adsorbate, the pore structure and surface chemistry property of adsorbent play dominant roles in adsorption kinetics behavior.

The diffusion and adsorption of gas molecular in coal is assumed to two stages with the bidisperse diffusion: surface diffusion in the micropore and pore diffusion in the meso/macropore (Cui et al., 2004; Wei et al., 2007). Thus, the pore structure of various coals before and after CO_2 exposure was studied and the results are listed in Table 4 (Wang et al., 2015). It can be found that both the meso/macropore volume and the micropore specific surface area of the coal after CO_2 exposure are less than that of the raw coal except ED coal. As reported by Clarkson and Bustin (1999b), pore volume distribution can significantly affect gas transport of coal. Moreover, Liu et al. (2015) also studied the effect of mesopore structure on the methane diffusion coefficient and found that the effective diffusion coefficient is proportional to the mesopore volume. Therefore, a decrease of meso/macropore volume may explain why high-pressure CO_2 exposure leads to a decline of meso/macropore diffusion coefficient of methane and CO_2 adsorption on coal as shown in Tables 2 and 3. With regard to the micropore structure dependence of adsorption kinetics behavior, gas diffusion and adsorption are mainly controlled by surface diffusion process (Zhang et al., 2011a). Thus, it is reasonable that the effective diffusion coefficient in micropore is proportional to the surface area of micropore. As can be seen in Table 4, the decreasing trend of the surface area of micropore is found for the coals after CO_2 exposure, which accounts for the decline in micropore apparent diffusivity as previously mentioned.

In addition, coal is abundant with functional groups mainly including oxygen-containing functional groups, nitrogen-containing functional groups and sulfur-containing functional groups, etc. Among them, the oxygen-containing functional groups are the most abundant species, which have great effect on the adsorption performance of coal. Numerous investigations have studied the effect of the oxygen-containing functional groups on methane and CO_2 adsorption on coal by using theory simulation or experimental method. Lu et al. (2015) employed density functional theory (DFT) and Grand Canonical Monte Carlo (GCMC) simulation to investigate the effect of some oxygen-containing functional groups (–OH, –COOH) on the competitive adsorption of a binary methane/CO_2 mixture on carbon materials. They found that oxygen-containing functional groups could enhance the selectivity of CO_2 over methane. Based on the results of molecular simulation, Liu and Wilcox (2013) found that the oxygen-containing functional

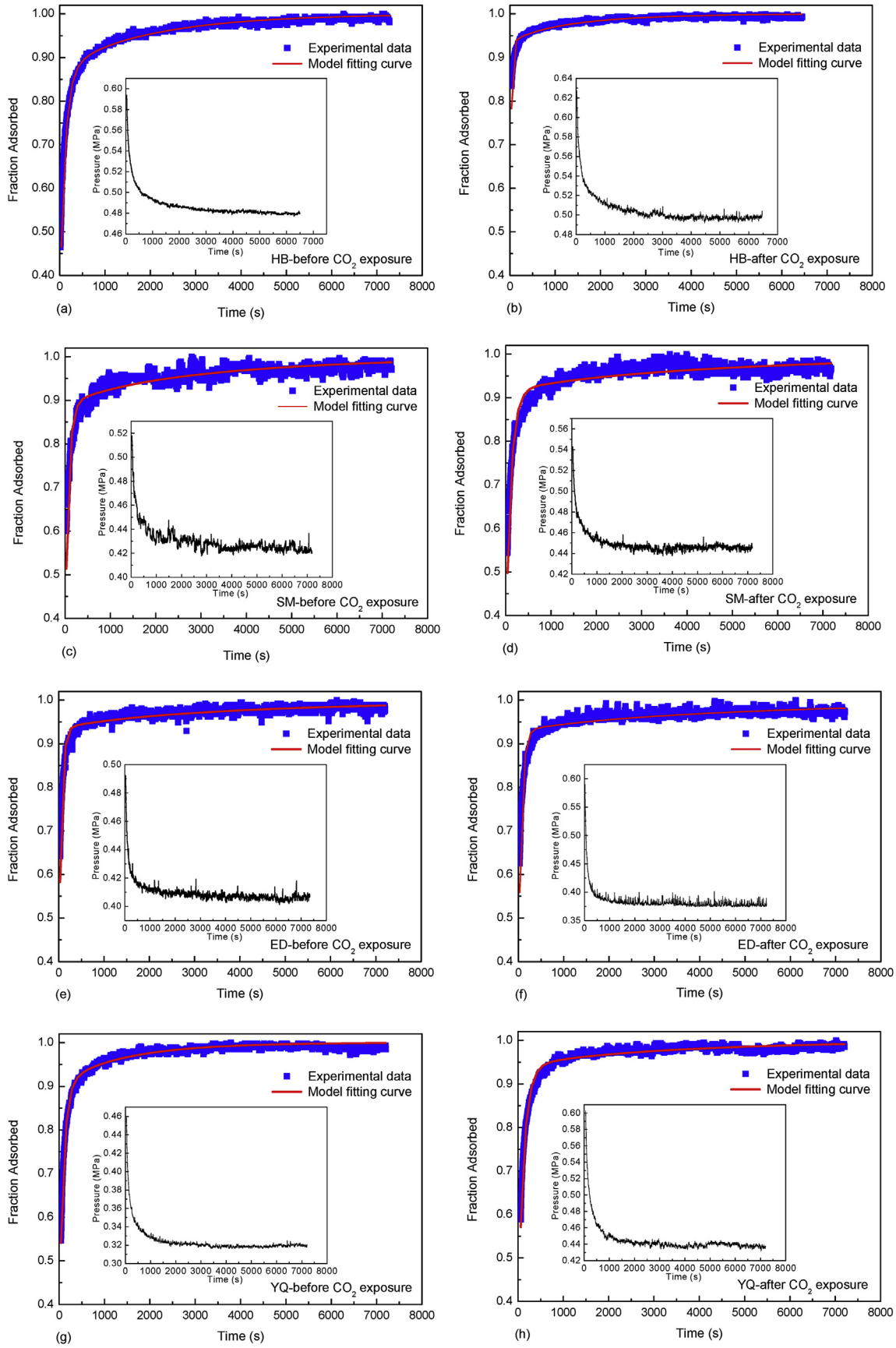

Fig. 4. Experimental and bidisperse model fitting curves of adsorption kinetics of methane adsorption on various coals.

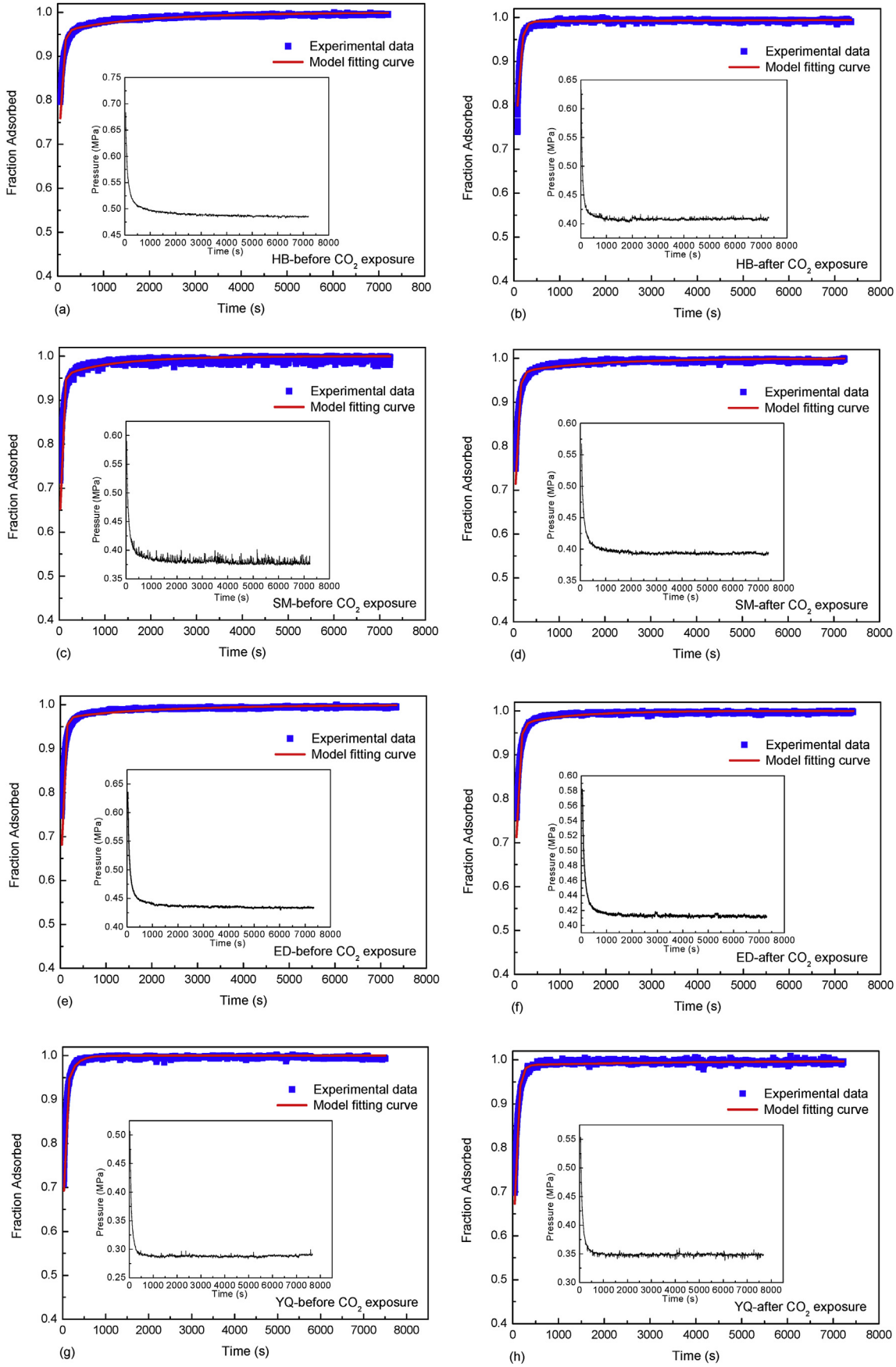

Fig. 5. Experimental and bidisperse model fitting curves of adsorption kinetics of CO_2 adsorption on various coals.

Table 2
Bidisperse model fitting results of methane adsorption on various coals.

Sample	State	D_{macro}/R^2_{macro} (s^{-1})	D_{micro}/R^2_{micro} (s^{-1})	β	R^2
HB	Before CO_2 exposure	8.80×10^{-4}	7.0×10^{-5}	0.81	0.9883
	After CO_2 exposure	4.83×10^{-4}	3.0×10^{-5}	0.91	0.9186
SM	Before CO_2 exposure	1.33×10^{-3}	3.0×10^{-5}	0.86	0.8904
	After CO_2 exposure	8.70×10^{-4}	2.0×10^{-5}	0.89	0.8922
ED	Before CO_2 exposure	1.71×10^{-3}	2.0×10^{-5}	0.92	0.9216
	After CO_2 exposure	1.50×10^{-3}	2.0×10^{-5}	0.91	0.8982
YQ	Before CO_2 exposure	1.10×10^{-3}	5.7×10^{-5}	0.86	0.9685
	After CO_2 exposure	8.00×10^{-4}	2.0×10^{-5}	0.92	0.9525

Table 3
Bidisperse model fitting results of CO_2 adsorption on various coals.

Sample	State	D_{macro}/R^2_{macro} (s^{-1})	D_{micro}/R^2_{micro} (s^{-1})	β	R^2
HB	Before CO_2 exposure	1.92×10^{-3}	5.0×10^{-5}	0.94	0.9547
	After CO_2 exposure	1.44×10^{-3}	3.9×10^{-5}	0.99	0.9558
SM	Before CO_2 exposure	2.73×10^{-3}	8.0×10^{-5}	0.94	0.9013
	After CO_2 exposure	1.84×10^{-3}	5.0×10^{-5}	0.95	0.9417
ED	Before CO_2 exposure	2.33×10^{-3}	8.0×10^{-5}	0.96	0.9326
	After CO_2 exposure	1.91×10^{-3}	6.0×10^{-5}	0.95	0.9477
YQ	Before CO_2 exposure	3.08×10^{-3}	5.7×10^{-4}	0.81	0.9550
	After CO_2 exposure	1.55×10^{-3}	2.0×10^{-5}	0.98	0.9696

Table 4
Micropore and meso/macropore parameters of coals before and after CO_2 exposure (Wang et al., 2015).

Sample	State	Meso/macropore parameters		Micropore parameters	
		S_{BET} ($m^2\ g^{-1}$)[a]	V_t ($cm^3\ g^{-1}$)[b]	S ($m^2\ g^{-1}$)[c]	V_t ($cm^3\ g^{-1}$)[d]
HB	Before CO_2 exposure	4.95	0.01589	162.49	0.03337
	After CO_2 exposure	5.21	0.01427	153.73	0.03206
SM	Before CO_2 exposure	5.42	0.00746	163.32	0.03100
	After CO_2 exposure	4.71	0.00619	153.32	0.02973
ED	Before CO_2 exposure	5.11	0.00676	134.15	0.02572
	After CO_2 exposure	5.15	0.00702	134.42	0.02560
YQ	Before CO_2 exposure	3.85	0.00612	173.39	0.03540
	After CO_2 exposure	3.60	0.00587	164.56	0.03312

[a] Brunauer, Emmett and Teller (BET) specific surface area.
[b] Single point adsorption total pore volume.
[c] Specific surface area obtained by Dubinin-Radushkevich (D-R) model.
[d] Total pore volume obtained by Dubinin-Radushkevich (D-R) model.

groups led to an increase in the density of adsorbed CO_2, especially for carboxyl functionalized graphitic slit pores. However, the oxygen-containing functional groups were not in favor of methane adsorption. Hao et al. (2013) and our previous work (Wang et al., 2015) reported that the oxygen-containing functional groups could enhance CO_2 adsorption but weaken methane adsorption on coal based on the experimental data. The different role of surface oxygen-containing functional groups on methane and CO_2 adsorption behavior on coal is mainly related to the partial charge distribution of the oxygen-containing functional groups (Liu and Wilcox, 2012, 2013). The oxygen atoms on the coal surface exhibit strong electronegativity, which have a high potential to donate electrons to the neighboring electron-deficient gas molecular and strengthen the interaction between CO_2 and coal surface. For methane adsorption, the oxygen-containing functional groups may block pore entrance and reduce dispersive interaction of methane with the pore surface of coal (Cuervo et al., 2008). The diffusion and adsorption process of methane and CO_2 within the pore structure of coal can be interpreted as a process of gas molecular adsorption constantly on the coal matrix surface and transport within the coal pores. Thus, the property and number of the sorption site may affect the adsorption kinetics behavior of gas molecular in coal. Thus, FTIR analysis was used to reveal the change of surface oxygen-containing functional groups of the coal after CO_2 exposure. The measured FTIR spectra of coals before and after CO_2 exposure are shown in Fig. S1, Supplementary data (Wang et al., 2015). Generally, the wave number ranging between 3100 and 3700 cm^{-1} is attributed to O–H stretching vibration. The spectra corresponding to 2800–3000 cm^{-1} are assigned to aliphatic C–H stretching vibration. The peak around wave number of 1600 cm^{-1} is assigned to C=C stretching vibration of aromatic rings. The main oxygen-containing functional groups including –C=O and –COOH can be found in the wave number ranging between 1500 and 1800 cm^{-1}. The peak around 1450 cm^{-1} is related to the bend vibrations of $-CH_2$ and $-CH_3$. The out-of-plane aromatic C–H vibration is observed between 700 and 900 cm^{-1}. In addition, it has pointed out that CO_2 exposure leads to a decrease of total oxygen-containing functional groups (Wang et al., 2015). In this work, the change of several kinds of the oxygen-containing functional groups related to methane and CO_2 adsorption was determined. Numerous works indicated that except hydroxyl (–OH), –C=O and –COOH contained in the selected region of 1800–1500 cm^{-1} as the main oxygen-containing functional groups have a greater contribution to gas adsorption behavior (Lu et al., 2015; Jin et al., 2014; Liu and Wilcox, 2013). The 1800-1500 cm^{-1} region includes aromatic C=C, aromatic ring stretch and oxygen-containing functional groups

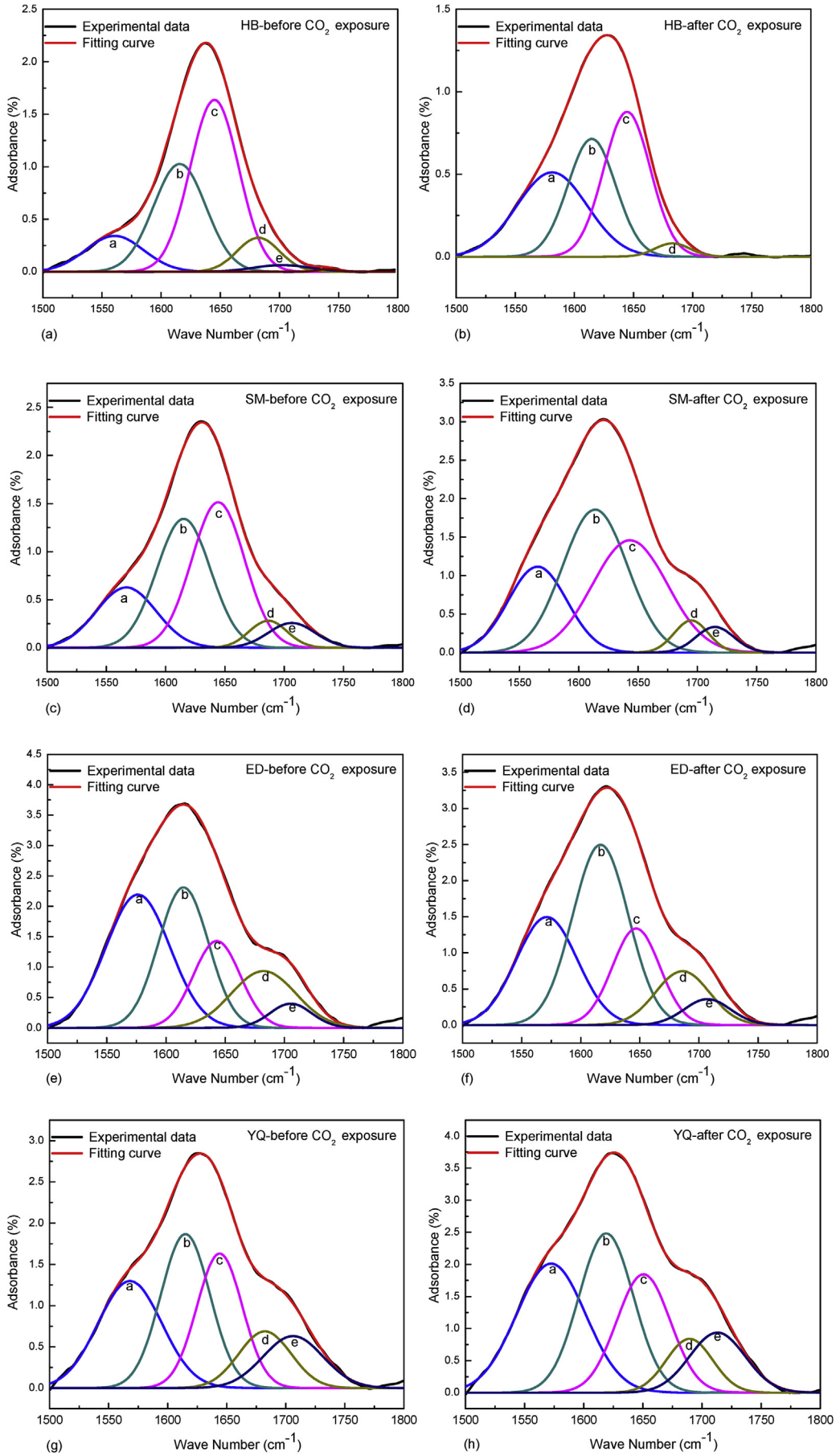

Fig. 6. Curve-fitted FTIR spectra of oxygen-containing functional groups on various coals.

Table 5
Assignment of peak position corresponding to wave number of 1800–1500 cm^{-1}.

Peak no.	Peak position (cm^{-1})	Assignment
a	1565	Aromatic ring stretch
b	1615	Aromatic C=C
c	1644	Highly conjugated C=O
d	1683	Conjugated C=O
e	1704	COOH

(−C=O, −COOH). Based on the previous literature (Chen et al., 2012; Geng et al., 2009), the 1800-1500 cm^{-1} is deconvoluted into five peaks using PeakFit software. The curve-fitted spectra of the raw and CO_2-exposed coal samples are shown in Fig. 6. The peak position and the relative abundance of oxygen-containing functional groups are listed in Table 5 and Table 6, respectively.

As can be seen in Table 6, the relative abundances of the oxygen-containing functional groups (C=O, -COOH) of the coals after CO_2 exposure are less than that of the raw coals, which means that CO_2 exposure leads to a decline of oxygen-containing functional groups. The decrease in the oxygen-containing functional groups is probably due to the extraction effect or the chemical reaction between supercritical CO_2 fluid and coal. Further demonstration of this point of view will be carried out in our future work. According to the aforementioned effect of oxygen-containing functional groups on methane and CO_2 adsorption on coal, it can be concluded that the decrease in oxygen-containing functional groups also contributes to the reduced diffusion rate of CO_2 in combination with the pore structure. For methane adsorption, although the decrease in oxygen-containing functional groups favors methane diffusion and adsorption, the influence of oxygen-containing functional groups may be inferior to the pore structure. Thus, the net result is that CO_2 exposure causes a reduced diffusion rate of methane within the coal structure.

In addition, as discussed in previous investigations (St. George and Barakat, 2001), coal matrix swelling induced by CO_2 sequestration may block the open channels and enhance the diffusion energy barrier of micropore and macropore of coal. Thus, swelling effect can also weaken the diffusion rate of fluid. Coal swelling is significant at higher pressure (Anggara et al., 2014; Day et al., 2008; Vishal et al., 2013). Therefore, under our experimental condition (P = 12 MPa), the decline of methane and CO_2 diffusion rate resulted from the coal matrix swelling cannot be ignored.

4.3. Implications for CO_2 sequestration in deep coal seams

Great attention has been paid to the complex interactions of coal and CO_2 which is a supercritical fluid under coal reservoir conditions. The coal property and pore structure play very important roles in methane and CO_2 transport and adsorption kinetics due to the specific interactions of CO_2 with coal. Based on the above analysis, CO_2 generally has a higher diffusion rate than methane for the test coal samples, which manifests that there is a strong selective transport of CO_2 over methane. The selective transport of CO_2 is favorable for the implication of CO_2 sequestration and methane recovery in coal seams.

It is acknowledged that gas transport properties are important for CO_2 sequestration and coalbed gas recovery. Previous studies have suggested that CO_2 exposure affects the change of coal property, which affects the diffusion behavior of methane and CO_2 on coal. As shown by our results, CO_2 exposure will decrease the methane and CO_2 diffusion and adsorption kinetics due to the change of coal property. However, displacement of methane by CO_2 injection is influenced by methane and CO_2 molecular diffusion and adsorption behavior. The strong decrease of methane and CO_2 diffusion coefficient due to CO_2 exposure may hinder CO_2 sequestration and methane recovery in coal seams. Moreover, under the reservoir conditions, the coal swelling resulted from the gas adsorption can reduce the reservoir permeability, consequently reducing the diffusivities, which is detrimental to the practical implementation of CO_2-ECBM.

For practical CO_2-ECBM, CO_2 injection mixed with an appropriate proportion of flue gas components (such as N_2) instead of pure CO_2 is recommended to mitigate the adverse effect of CO_2 exposure. Additionally, it is also reported that CO_2 injection with a proportion of N_2 can mitigate the reduction in permeability of coal seams due to matrix swelling (Pini et al., 2009). Investigation on the coalbed methane recovery by injection CO_2/N_2 mixture will be performed to demonstrate this proposal.

5. Conclusion

In this work, four coals were chosen to address the effect of high-pressure CO_2 exposure on the adsorption kinetics of methane and CO_2 at the conditions of T = 45 °C, and P = 0.41 MPa. The bidisperse model was applied to describe the diffusion behavior of methane and CO_2 on coal. The relevant conclusions can be summarized as follows:

1) The bidisperse model can describe the diffusion behavior of methane and CO_2 on coals before and after CO_2 exposure. 2) Compared with the raw coal, there exists a significant decrease in the diffusion rate of methane and CO_2 on coals after CO_2 exposure. 3) The results of the FTIR analysis show that the CO_2 exposure has a significant impact on the decrease of the oxygen-containing functional groups. Moreover, pore morphology analyses show that the meso/macropore volume and the micropore surface area of coal after CO_2 exposure decrease slightly. Additionally, at high pressure, the coal swelling resulted from the gas adsorption can reduce the coal permeability, which will drop the diffusivity. The above mentioned factors may be responsible for the roles of CO_2 exposure on methane and CO_2 diffusion behavior on coal. 4) Based on the decrease of the diffusion coefficient from the CO_2 exposure, it is deduced that primarily injected high-pressure CO_2 may hinder CO_2 sequestration and methane recovery in the target coal seams. Thus, the recommendation of injection of CO_2 mixed with an appropriate proportion of flue gas components, such as N_2, instead of pure CO_2

Table 6
Relative abundance of oxygen-containing functional groups and aromatic structure, %.

Sample	Highly conjugated C=O		Conjugated C=O		COOH		Aromatic C=C		Aromatic ring stretch	
	*	**	*	**	*	**	*	**	*	**
HB	50.13	36.04	2.99	2.47	2.84	–	31.90	30.05	12.14	31.44
SM	37.74	33.98	5.00	4.42	5.66	3.93	33.97	37.43	17.63	20.24
ED	16.78	18.05	15.06	11.46	4.16	4.73	28.92	39.82	35.08	25.94
YQ	23.06	21.70	11.16	8.54	11.74	11.42	28.54	29.67	25.50	28.67

*before CO_2 exposure. **after CO_2 exposure.

is of potential to enhance CO_2 sequestration and methane recovery. Further demonstration of this proposal will be carried out on the study of coalbed methane recovery by injection CO_2/N_2 mixture.

Acknowledgment

This work is conducted with funding from the project supported by the National Natural Science Foundation of China (Grant No. 41302132), Introduced Talents Foundation of Kunming University of Science and Technology (Grant No. KKSY201205160), Science Foundation of the Education Department of Yunnan Province (Grant No. 2015Y063), Analysis and Measurement Foundation of Kunming University of Science and Technology (Grant No. 20140826, 20150373) and Training Program of Innovation and Entrepreneurship for Undergraduates of Yunnan Province (Grant No. 201510674042).

Appendix A. Supplementary data

Supplementary data related to this article can be found at http://dx.doi.org/10.1016/j.jngse.2016.07.042.

References

Anggara, F., Sasaki, K., Rodrigues, S., Sugai, Y., 2014. The effect of megascopic texture on swelling of a low rank coal in supercritical carbon dioxide. Int. J. Coal Geol. 125 (0), 45–56.
Bhowmik, S., Dutta, P., 2013. Adsorption rate characteristics of methane and CO_2 in coal samples from Raniganj and Jharia coalfields of India. Int. J. Coal Geol. 113, 50–59.
Busch, A., Gensterblum, Y., Krooss, B.M., Littke, R., 2004. Methane and carbon dioxide adsorption-diffusion experiments on coal: upscaling and modeling. Int. J. Coal Geol. 60 (2–4), 151–168.
Cao, X.Y., Mastalerz, M., Chappell, M.A., Miller, L.F., Li, Y., Mao, J.D., 2011. Chemical structures of coal lithotypes before and after CO_2 adsorption as investigated by advanced solid-state C-13 nuclear magnetic resonance spectroscopy. Int. J. Coal Geol. 88 (1), 67–74.
Charrière, D., Pokryszka, Z., Behra, P., 2010. Effect of pressure and temperature on diffusion of CO_2 and CH_4 into coal from the Lorraine basin (France). Int. J. Coal Geol. 81 (4), 373–380.
Chen, Y.Y., Mastalerz, M., Schimmelmann, A., 2012. Characterization of chemical functional groups in macerals across different coal ranks via micro-FTIR spectroscopy. Int. J. Coal Geol. 104, 22–33.
Clarkson, C.R., Bustin, R.M., 1999a. The effect of pore structure and gas pressure upon the transport properties of coal: a laboratory and modeling study. 2. adsorption rate modeling. Fuel 78 (11), 1345–1362.
Clarkson, C.R., Bustin, R.M., 2000. Binary gas adsorption/desorption isotherms: effect of moisture and coal composition upon carbon dioxide selectivity over methane. Int. J. Coal Geol. 42 (4), 241–271.
Clarkson, C.R., Bustin, R.M., 1999b. The effect of pore structure and gas pressure upon the transport properties of coal: a laboratory and modeling study. 1. isotherms and pore volume distributions. Fuel 78 (11), 1333–1344.
Clarkson, C.R., Bustin, R.M., Levy, J.H., 1997. Application of the mono/multilayer and adsorption potential theories to coal methane adsorption isotherms at elevated temperature and pressure. Carbon 35 (12), 1689–1705.
Cuervo, M.R., Asedegbega-Nieto, E., Díaz, E., Ordóñez, S., Vega, A., Dongil, A.B., Rodríguez-Ramos, I., 2008. Modification of the adsorption properties of high surface area graphites by oxygen functional groups. Carbon 46 (15), 2096–2106.
Cui, X.J., Bustin, R.M., Dipple, G., 2004. Selective transport of CO_2, CH_4, and N_2 in coals: insights from modeling of experimental gas adsorption data. Fuel 83 (3), 293–303.
Day, S., Fry, R., Sakurovs, R., 2008. Swelling of Australian coals in supercritical CO_2. Int. J. Coal Geol. 74 (1), 41–52.
Do, D.D., Do, H.D., 2003. Adsorption of supercritical fluids in non-porous and porous carbons: analysis of adsorbed phase volume and density. Carbon 41 (9), 1777–1791.
Gan, H., Nandi, S.P., Walker Jr., P.L., 1972. Nature of the porosity in American coals. Fuel 51 (4), 272–277.
Gathitu, B.B., Chen, W.Y., McClure, M., 2009. Effects of coal interaction with supercritical CO_2: physical structure. Ind. Eng. Chem. Res. 48 (10), 5024–5034.
Geng, W., Nakajima, T., Takanashi, H., Ohki, A., 2009. Analysis of carboxyl group in coal and coal aromaticity by Fourier transform infrared (FT-IR) spectrometry. Fuel 88 (1), 139–144.
Giroux, L., Charland, J.-P., MacPhee, J.A., 2006. Application of thermogravimetric Fourier transform infrared spectroscopy to the analysis of oxygen functional groups in coal. Energy Fuels 20 (5), 1988–1996.
Goodman, A.L., Favors, R.N., Larsen, J.W., 2006. Argonne coal structure rearrangement caused by sorption of CO_2. Energy Fuels 20 (6), 2537–2543.
Green, U., Aizenstat, Z., Gieldmeister, F., Cohen, H., 2011. CO_2 adsorption inside the pore structure of different rank coals during low temperature oxidation of open air coal stockpiles. Energy Fuels 25 (9), 4211–4215.
Gruszkiewicz, M.S., Naney, M.T., Blencoe, J.G., Cole, D.R., Pashin, J.C., Carroll, R.E., 2009. Adsorption kinetics of CO_2, CH_4, and their equimolar mixture on coal from the Black Warrior Basin, West-Central Alabama. Int. J. Coal Geol. 77 (1–2), 23–33.
Hao, S.X., Wen, J., Yu, X.P., Chu, W., 2013. Effect of the surface oxygen groups on methane adsorption on coals. Appl. Surf. Sci. 264, 433–442.
Harpalani, S., Prusty, B.K., Dutta, P., 2006. Methane/CO_2 sorption modeling for coalbed methane production and CO_2 Sequestration. Energy Fuels 20 (4), 1591–1599.
Huang, X., Chu, W., Sun, W., Jiang, C., Feng, Y., Xue, Y., 2014. Investigation of oxygen-containing group promotion effect on CO_2-coal interaction by density functional theory. Appl. Surf. Sci. 299 (0), 162–169.
Jin, D.L., Lu, X.Q., Zhang, M.M., Wei, S.X., Zhu, Q., Shi, X.F., Shao, Y., Wang, W.L., Guo, W.Y., 2014. The adsorption behaviour of CH_4 on microporous carbons: effects of surface heterogeneity. Phys. Chem. Chem. Phys. 16 (22), 11037–11046.
Kolak, J.J., Burruss, R.C., 2014. The use of solvent extractions and solubility theory to discern hydrocarbon associations in coal, with application to the coal-supercritical CO_2 system. Org. Geochem 73 (0), 56–69.
Kolak, J.J., Burruss, R.C., 2006. Geochemical investigation of the potential for mobilizing non-methane hydrocarbons during carbon dioxide storage in deep coal beds. Energy Fuels 20 (2), 566–574.
Kolak, J.J., Hackley, P.C., Ruppert, L.F., Warwick, P.D., Burruss, R.C., 2015. Using ground and intact coal samples to evaluate hydrocarbon fate during supercritical CO_2 injection into coal beds: effects of particle size and coal moisture. Energy Fuels 29 (8), 5187–5203.
Li, W., Liu, H.F., Song, X.X., 2015. Multifractal analysis of Hg pore size distributions of tectonically deformed coals. Int. J. Coal Geol. 144–145, 138–152.
Lin, W., Tang, G.Q., Kovscek, A.R., 2008. Sorption-induced permeability change of coal during gas-injection processes. SPE Reserv. Eval. Eng. 11 (4), 792–802.
Lindzen, R.S., 1997. Can increasing carbon dioxide cause climate change? Proc. Natl. Acad. Sci. 94 (16), 8335–8342.
Liu, H.H., Mou, J.H., Cheng, Y.P., 2015. Impact of pore structure on gas adsorption and diffusion dynamics for long-flame coal. J. Nat. Gas. Sci. Eng. 22, 203–213.
Liu, Y.Y., Wilcox, J., 2012. Molecular simulation of CO_2 adsorption in micro- and mesoporous carbons with surface heterogeneity. Int. J. Coal Geol. 104, 83–95.
Liu, Y.Y., Wilcox, J., 2013. Molecular simulation studies of CO_2 adsorption by carbon model compounds for carbon capture and sequestration applications. Environ. Sci. Technol. 47, 95–101.
Lu, X.Q., Jin, D.L., Wei, S.X., Zhang, M.M., Zhu, Q., Shi, X.F., Deng, Z.G., Guo, W.Y., Shen, W.Z., 2015. Competitive adsorption of a binary CO_2-CH_4 mixture in nanoporous carbons: effects of edge-functionalization. Nanoscale 7 (3), 1002–1012.
Mastalerz, M., Gluskoter, H., Rupp, J., 2004. Carbon dioxide and methane sorption in high volatile bituminous coals from Indiana, USA. Int. J. Coal Geol. 60 (1), 43–55.
Mastalerz, M., Solano-Acosta, W., Schimmelmann, A., Drobniak, A., 2009. Effects of coal storage in air on physical and chemical properties of coal and on gas adsorption. Int. J. Coal Geol. 79 (4), 167–174.
Mazumder, S., Wolf, K.H., 2008. Differential swelling and permeability change of coal in response to CO_2 injection for ECBM. Int. J. Coal Geol. 74 (2), 123–138.
Nie, B.S., Liu, X.F., Yang, L.L., Meng, J.Q., Li, X.C., 2015. Pore structure characterization of different rank coals using gas adsorption and scanning electron microscopy. Fuel 158, 908–917.
Orr Jr., F.M., 2009. Onshore geologic storage of CO_2. Science 325 (5948), 1656–1658.
Pan, Z.J., Connell, L.D., Camilleri, M., Connelly, L., 2010. Effects of matrix moisture on gas diffusion and flow in coal. Fuel 89 (11), 3207–3217.
Pini, R., Ottiger, S., Burlini, L., Storti, G., Mazzotti, M., 2009. Role of adsorption and swelling on the dynamics of gas injection in coal. J. Geophys. Res. 114 http://dx.doi.org/10.1029/2008JB005961.
Prusty, B.K., 2008. Sorption of methane and CO_2 for enhanced coalbed methane recovery and carbon dioxide sequestration. J. Nat. Gas. Chem. 17 (1), 29–38.
Ruckenstein, E., Vaidyanathan, A.S., Youngquist, G.R., 1971. Sorption by solids with bidisperse pore structures. Chem. Eng. Sci. 26 (9), 1305–1318.
Sakurovs, R., Day, S., Weir, S., 2009. Causes and consequences of errors in determining sorption capacity of coals for carbon dioxide at high pressure. Int. J. Coal Geol. 77 (1–2), 16–22.
Shi, J.Q., Durucan, S., Shimada, S., 2014. How gas adsorption and swelling affects permeability of coal: a new modelling approach for analysing laboratory test data. Int. J. Coal Geol. 128, 134–142.
Shieh, J., Chung, T., 1999. Gas permeability, diffusivity, and solubility of poly (4-vinylpyridine) film. J. Polym. Sci. B Polym. Phys. 37 (20), 2851–2861.
Siemons, N., Busch, A., 2007. Measurement and interpretation of supercritical CO_2 sorption on various coals. Int. J. Coal Geol. 69 (4), 229–242.
Siriwardane, H.J., Gondle, R.K., Smith, D.H., 2009. Shrinkage and swelling of coal induced by desorption and sorption of fluids: theoretical model and interpretation of a field project. Int. J. Coal Geol. 77 (1–2), 188–202.
Smith, D.M., Williams, F.L., 1984. Diffusion models for gas production from coals: application to methane content determination. Fuel 63 (2), 251–255.
Smith, D.M., 1982. Methane Diffusion and Desorption in Coal (Ph. D. thesis). University of New Mexico, U.S.A.
Span, R., Wagner, W., 1996. A new equation of state for carbon dioxide covering the

fluid region from the triple-point temperature to 1100 K at pressures up to 800 MPa. J. Phys. Chem. Ref. Data 25 (6), 1509–1596.
St George, J.D., Barakat, M.A., 2001. The change in effective stress associated with shrinkage from gas desorption in coal. Int. J. Coal Geol. 45 (2–3), 105–113.
Viete, D.R., Ranjith, P.G., 2007. The mechanical behaviour of coal with respect to CO_2 sequestration in deep coal seams. Fuel 86 (17–18), 2667–2671.
Vishal, V., Ranjith, P.G., Singh, T.N., 2013. CO_2 permeability of Indian bituminous coals: implications for carbon sequestration. Int. J. Coal Geol. 105, 36–47.
Wagner, W., Span, R., 1993. Special equations of state for methane, argon, and nitrogen for the temperature range from 270 to 350 K at pressures up to 30 MPa. Int. J. Thermophys. 14 (4), 699–725.
Wang, Q.Q., Zhang, D.F., Wang, H.H., Jiang, W.P., Wu, X.P., Yang, J., Huo, P.L., 2015. Influence of CO_2 exposure on high-pressure methane and CO_2 adsorption on various rank coals: implications for CO_2 sequestration in coal seams. Energy Fuels 29 (6), 3785–3795.
Wei, X.R., Wang, G.X., Massarotto, P., Golding, S.D., Rudolph, V., 2007. Numerical simulation of multicomponent gas diffusion and flow in coals for CO_2 enhanced coalbed methane recovery. Chem. Eng. Sci. 62 (16), 4193–4203.
White, C.M., Smith, D.H., Jones, K.L., Goodman, A.L., Jikich, S.A., LaCount, R.B., DuBose, S.B., Ozdemir, E., Morsi, B.I., Schroeder, K.T., 2005. Sequestration of carbon dioxide in coal with enhanced coalbed methane recovery-a review. Energy Fuels 19 (3), 659–724.
Wong, S., Law, D., Deng, X.H., Robinson, J., Kadatz, B., Gunter, W.D., Ye, J.P., Feng, S.L., Fan, Z.P., 2007. Enhanced coalbed methane and CO_2 storage in anthracitic coals-micro-pilot test at South Qinshui, Shanxi, China. Int. J. Greenh. Gas. Control 1 (2), 215–222.
Yang, R.T., 2003. Adsorbents: Fundamentals and Applications. John Wiley and Sons Inc., New York.
Yao, Y.B., Liu, D.M., Xie, S.B., 2014. Quantitative characterization of methane adsorption on coal using a low-field NMR relaxation method. Int. J. Coal Geol. 131 (0), 32–40.
Zhang, D.F., Cui, Y.J., Li, S.G., Song, W.L., Lin, W.G., 2011a. Adsorption and diffusion behaviors of methane and carbon dioxide on various rank coals. J. China Coal Soc. 36 (10), 1693–1698 (in Chinese with English abstract).
Zhang, D.F., Cui, Y.J., Liu, B., Li, S.G., Song, W.L., Lin, W.G., 2011b. Supercritical pure methane and CO_2 adsorption on various rank coals of China: experiments and Modeling. Energy Fuels 25 (4), 1891–1899.
Zhang, D.F., Gu, L.L., Li, S.G., Lian, P.C., Tao, J., 2013a. Interactions of supercritical CO_2 with coal. Energy Fuels 27 (1), 387–393.
Zhang, D.F., Gu, L.L., Li, S.G., Lian, P.C., Tao, J., 2013b. Error analyses in volumetric method for measuring methane and CO_2 adsorption on coal. Int. J. Glob. Warm. 5 (2), 197–209.
Zhang, D.F., Li, S.G., Cui, Y.J., Song, W.L., Lin, W.G., 2011c. Displacement behavior of methane adsorbed on coal by CO_2 injection. Ind. Eng. Chem. Res. 50 (14), 8742–8749.
Zhou, F.D., Hussain, F., Cinar, Y., 2013. Injecting pure N_2 and CO_2 to coal for enhanced coalbed methane: experimental observations and numerical simulation. Int. J. Coal Geol. 116, 53–62.